Hindawi
Wireless Communications and Mobile Computing
Volume 2019, Article ID 5473923, 13 pages
https://doi.org/10.1155/2019/5473923

Research Article

Optical Wireless Network Design for Off-Body-Sensor Based Monitoring

T. B. Hoang, S. Sahuguede, and A. Julien-Vergonjanne

University of Limoges, CNRS, XLIM UMR 7252, F-87000 Limoges, France

Correspondence should be addressed to A. Julien-Vergonjanne; anne@ensil.unilim.fr

Received 28 March 2019; Revised 2 July 2019; Accepted 22 July 2019; Published 2 September 2019

Guest Editor: Ian Cleland

In this article, we propose an all-optical bidirectional wireless communication system for off-body sensor communication. Optical technology uses infrared (IR) for uplinks and visible light communication (VLC) for downlinks. From numerical simulations, we discuss the impact of body sensor positions on IR and VLC channels. Our goal is to evaluate the possibilities of using optical technology to transmit sensor data for extreme positions such as the ankle, for which the presence of the body creates blockages. In addition, we also consider the variations in orientation of transceivers due to random mobility of body parts during normal movement. Based on a statistical approach, we evaluate performance in terms of outage probability using channel impulse response sets corresponding to the studied scenario, which is health monitoring. Considering a given quality of service, we address trade-offs related to emitting power and data rate. We discuss the results regarding sensor node position and body reflectivity specifically for ankle sensors, corresponding to an extreme but realistic position in the health-monitoring context.

1. Introduction

Optical wireless communications (OWCs) have been intensively explored in recent decades, particularly in the visible domain [1–6]. This is related to the penetration of LEDs for lighting, the switching properties of which also make it possible to use them for communication functions. Such smart lighting offers many benefits, including no license requirements, high bandwidth, and no electromagnetic interference. This technology is applied today in a wide range of use cases including healthcare devices in hospitals and homes and medical body sensor networks [7]. The use of classical radiofrequency (RF) technologies can be limited in some environments because of potential interference with sensitive devices. For example, IEC 60601-1-2 standard [8] recommends a minimum separation distance between medical electrical equipment and RF communications gateways to avoid performance degradation. OWC technology can be deployed as an alternative to ensure adequate performance, avoiding interference. In addition, since optical rays are confined to the environment, this easily permits avoiding signal interception from outside of the room and also deploying the same device in neighboring rooms. Besides, OWC appears as one of the alternatives to reduce pressure on the already overloaded RF spectrum because of a growing number of connected devices [9] especially in indoor environment. One limitation when using OWC is about optical power, which has to respect eye safety standards. Infrared LED power is generally limited according to the laser safety standard [10]. However, this standard is very restrictive for most noncoherent light sources. Thus, standard for conventional lamps and LEDs [11] is also classically used.

OWC systems applied in the medical field have been studied for several years. To replace cables between medical sensors and monitoring stations, IR links are a solution that is already adopted. International standards define communications services and protocols that are consistent with IrDA specifications and are optimized for portable devices near the patient such as bedside medical ones [12]. However, this is for static point-to-point communications. Some works have considered IR transmissions between a mobile patient equipped with connected sensor and an access point in the environment for both classical indoor

OWC schemes, that is, line-of-sight (LOS) and diffuse systems [2].

In [13], LOS configuration based on directed optical propagation has been studied for a sensor on the top of the head, which is quite limited regarding practical case. It was shown that the misalignment of transmitter and receiver can significantly increase the BER, and a tracking system was required. In diffuse scenario, the communication link is established thanks to the optical reflections over the environment. This scheme is investigated in [14] where the IR sensor is located at the belt pointing towards the floor. The authors in [15] experimentally confirmed the potentialities of IR system based on the diffuse configuration for mobile patient monitoring. Besides, a custom-made wearable device is presented in [16], which allows OWC-based transmission of accelerometer data in the context of physical activity supervision of poststroke patients in hospital. On the other hand, Alyan and Aljunid [17] and Chevalier et al. [18] have proposed multiple access schemes based on CDMA spreading codes. In [17], the access point is classically located on the ceiling, whereas Chevalier et al. [18] considered that all IR nodes were on-body, exploiting only diffuse reflections over the patient environment to establish transmissions. However, in all these works, the body carrying the sensors has not been taken into account. Our first contribution in this study is to analyze the IR uplink channel behavior regarding both user movement and sensor location on the body.

With the development of new possibilities offered by visible domain, many studies also deal with the potentialities of VLC related to health monitoring. The majority of works have proposed VLC uplink use to transmit health data from sensors. The studied configurations are generally static as in [19–22] and concern ECG and EEG data. In [23, 24], an image sensor is used for the visible signal reception. The receiver is either located on the ceiling [23] or included in the smartphone [24]. In these cases, mobile monitoring is investigated, but the performance is limited in terms of distance and data rates. Another limitation of VLC uplink is due to potential discomfort when a visible signal is emitted from sensors worn by a user. VLC is more suitable for downlinks when illumination and communication are coupled. Experimental works are reported in [25, 26] using visible LOS configurations to transmit health data. However, VLC challenges related to mobility are not addressed.

Therefore, we also present the study of downlink visible channel with regard to the body's optical properties and orientation changes in the transmitters resulting from patient movements. Based on IR and visible channel numerical analysis, our goal is to determine the overall performance of both optical links, taking into account all the impacting parameters.

The rest of this paper is structured as follows: Section 2 shows relative work; Section 3 introduces the investigated scenario and Section 4 the approach we follow to study IR and visible channel behavior; Section 5 presents the performance results and discussion; and Section 6 closes with conclusions.

2. Related Works

In [27], a mobile IR/VLC scenario was studied, but for a sensor position on the shoulder so that the behavior of the IR channel is not affected by the body presence. Therefore, body has not been modeled for the analysis of the IR channel. These results cannot be applied when the sensor is positioned at other places on the body. Indeed, in this case, the presence of the body can induce blockages and all the more so that the patient is mobile.

Published works have mainly addressed scenarios where optical devices are located on the upper body, e.g., as ECG sensors [19]. However, several use cases such as activity monitoring or rehabilitation applications need the sensor nodes to be positioned at the knee and/or ankle [28]. In this case, the effect of the human body on optical wireless transmission can be significant. This has been experimentally verified in [29] for a sensor located at the ankle, justifying the need for accurate and realistic models in order to explore performance in this context. Therefore, one of the main challenges remains the limitation of performance due to sensor positioning on the patient in particular at positions below the knee, for infrared and visible channels.

In this paper, we investigate an optical wireless body sensor scenario by considering different positions of the sensor on the patient, not only the shoulder but also particularly the ankle, which is an extreme but realistic use case position. In addition, to introduce realistic scenarios, we model changes in the transceivers' orientation due to random mobility and movements of the patient. The bidirectional all-optical scenario considers both an infrared emitter node and a visible light receiver. The infrared transmitter is located at a fixed position on the body of a patient, and the VLC receiver is held in the hand of either the patient or another person in another room. IR receivers and VLC transmitters are included in ceiling luminaires, as in [27].

3. System Description

To discuss the potentialities of an all-optical solution for body sensor communication, we consider a lighting system, which is a classical flat, square LED panel ready for VLC with four identical IR receivers placed at the corners and oriented in such a way able to enlarge coverage (Figure 1). VLC is used for the downlink since it permits combining illumination and communication functions. On the contrary, it is worth using IR uplink in order to avoid any visual discomfort.

An IR single-input multiple-output (SIMO) uplink is established between the sensor ($T_{x\text{-}IR}$) positioned on the body and the IR receivers ($R_{x\text{-}IR\text{-}i}$ with $i = 1$ to 4) included in the luminaire as shown in Figure 1(a). The visible communication downlink is described in Figure 1(b) where the emitter ($T_{x\text{-}VLC}$) is the LED luminaire and the receiver ($R_{x\text{-}VLC}$) is integrated, for example, into a tablet. This bidirectional scheme can be considered in the same room, for example, when the patient himself wears the tablet. The system can also be deployed in several

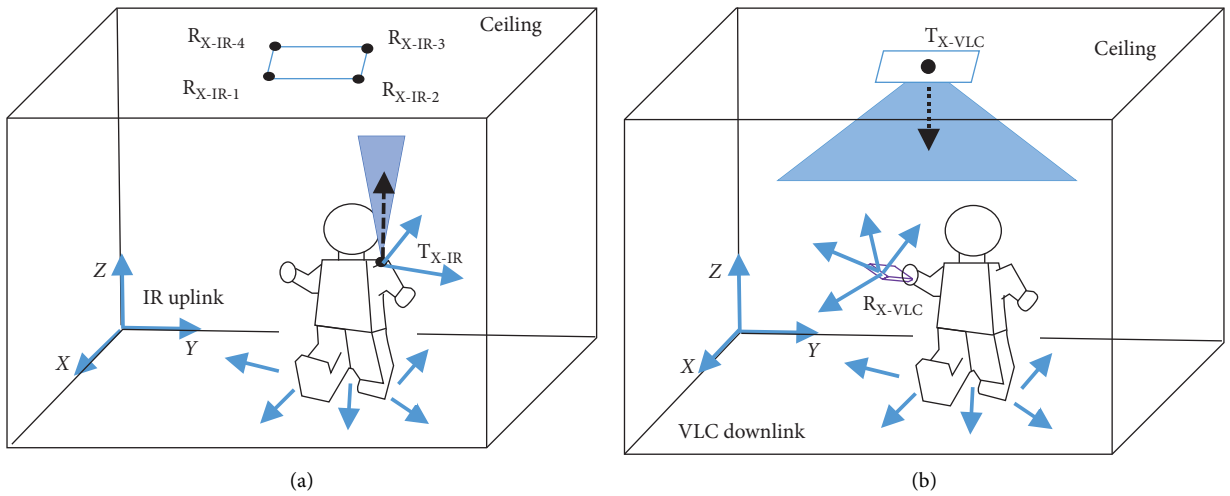

Figure 1: System description: (a) infrared (IR) uplink; (b) visible downlink.

neighboring rooms. Power line communication (PLC) technology can be used as example to interconnect the different luminaires and transmit the data to them [30]. In this case, the patient is only wearing the IR transmitter and it may be a medical staff in another room receiving on their tablet information about the patient's status.

In this work, we do not study the processing performed between the sensor data collected at the luminaire and the information transmitted to the tablet. We focus on IR and VLC links regarding both user movement and sensor location on the body. In particular, we explore the case of sensors for motion monitoring applications. It can be accelerometer, gyroscope, and magnetometer to track the patient's gait, postures, and movements. They are generally positioned at the lower limbs on the knee and ankle. Therefore, body can affect transmission robustness by blocking some links during the movement. Besides, data rate is below Mbps and is not the main challenge [7].

For both links, the emitter is supposed to have a Lambertian radiation pattern, whose directivity is characterized by the half-power angle $\varphi_{1/2}$ or the m order, linked by [2]

$$m = -\frac{\ln(2)}{\ln(\cos(\varphi_{1/2}))}. \quad (1)$$

3.1. VLC Downlink Description. The smart panel is in a central position on the ceiling of a room of dimensions $(6.7 \times 6.6 \times 2.8)$ m^3 (*length*, *width*, *height*). It has an area of 0.36 m^2 and is situated 20 cm from the ceiling. We assume that it is possible to control the brightness of a LED emitter placed at the center of the panel, directed towards the ground. In the rest of the study, the transmitter is characterized by the average optical power transmitted by the LED $P_{t\text{-}VLC}$, which is linked to the light level [3–6]. In addition, we suppose that the LED radiation pattern is a Lambertian one with an m order equal to 1 that corresponds to a half-power angle $\varphi_{1/2} = 60^\circ$ [4–6].

The patient moves randomly in the room while holding a device equipped with a VLC receiver. We consider that this device is held at a distance of 20 cm in front of the body and at a fixed height of 1.2 m from the ground. Patient positions anywhere in the room induce nondirected line-of-sight (LOS) links related to the optical properties of the environment. In addition, the patient's body can cause blockages depending on its reflectivity properties. As mobility also implies body movements and consequently receiver orientation variations, we define azimuthal and polar angles, respectively, as φ and θ, as illustrated in Figure 2, whose values are uniformly and randomly chosen within $\varphi \in [0, 2\pi]$ and $\theta \in [0, \pi/3]$ with a step of $\pi/6$. Actually, we limit the variation to $\pi/3$ because we suppose that the user carrying the tablet consults the results, which means that we do not consider that the tablet is directed towards the ground for example.

The parameters of the VLC downlink are given in Table 1, together with the values used for responsivity R, field-of-view (FOV), and photodetector physical area, which are typical values for VLC receivers.

3.2. IR Uplink Description. The patient carries an infrared emitter for the transmission of medical sensor data. Therefore, we consider IR emitter mobility and the effect related to the position of the sensor on the body, defined by the height H_T of the emitter from the floor as shown in Figure 3.

For this purpose, we consider a range of H_T values between 0.2 m, corresponding to a sensor at the ankle, and 1.7 m for a position near the top of the head (Figure 4). We do not consider values upper than the height of the body since the transmitter is supposed to be worn by a person. Furthermore, we consider a Lambertian radiation pattern for the IR source, with an optimal m order equal to 2, corresponding to a half-power angle of 45°. This is the optimal value for nondirected indoor transmissions, as shown previously by several authors [31, 32]. For such a scenario, the received IR power is due to the power from the LOS path and from reflected paths over the room surfaces. In addition, the body can have a more or less significant blocking effect depending on the position of the emitter.

Patient mobility and movements also induce random changes in IR emitter orientation. As the emitter is located

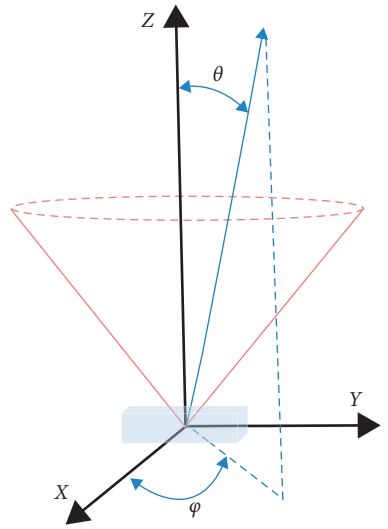

Figure 2: Definition of azimuthal and polar angles.

Table 1: VLC downlink parameters.

	Parameter	Value
$T_{X\text{-}VLC}$	Coordinates $[x, y, z]$	[3.35, 3.3, 2.8] (m)
	Half-power angle $\varphi_{1/2}$	60°
$R_{X\text{-}VLC}$	Height of receiver from the floor	1.2 m
	Distance from the body	20 cm in front of the body
	Polar angle θ	Random in $[0, \pi/3]$, with a step of $\pi/6$
	Azimuthal angle φ	Random in $[0, 2\pi]$, with a step of $\pi/6$
	Field-of-view (FOV)	65°
	Physical surface area	1 cm^2
	Responsivity	1 A/W

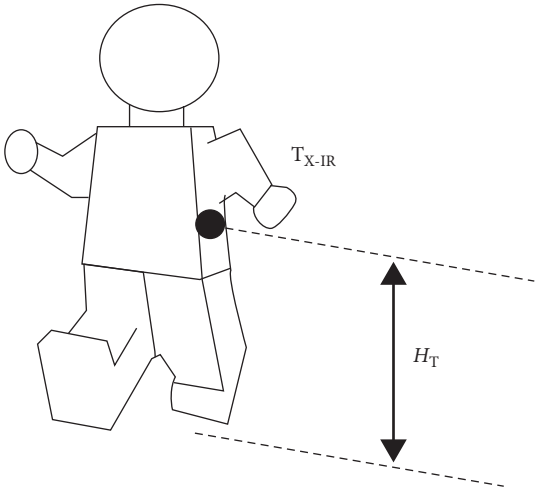

Figure 3: Definition of height of IR emitter.

on the body, we restrict the variation range of the azimuthal angle to $\varphi \in [0, \pi]$. The polar angle values are the same as previously reported, i.e., $\theta \in [0, \pi/3]$.

To improve IR coverage with regard to mobility, we use four identical IR receivers located at each corner of the lighting panel. Previous studies have shown that their

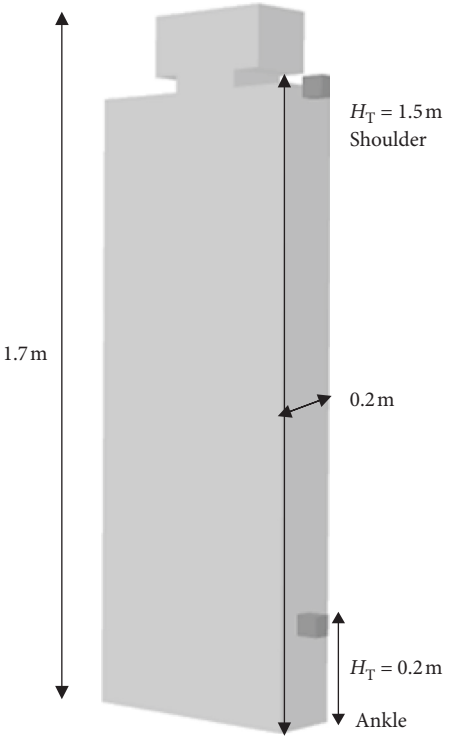

Figure 4: Definition of body model.

optimal orientation is 45° [31]. To exploit diversity, various combining techniques can be used such as selection combining (SC), maximum ratio combining (MRC), or equal gain combining (EGC) [33]. Here, we use the simplest one, which is switching combining (SwC), selecting the information only once whether one or several receivers correctly receive it. Table 2 lists the parameters for IR uplink including the main features of IR photodetectors.

4. Optical Channel Analysis

One of the main parameters of the optical channel is the DC gain, which determines the achievable signal-to-noise ratio for a fixed transmitter power. It is defined as

$$H_0 = \int_{-\infty}^{+\infty} h(t)dt, \tag{2}$$

where $h(t)$ represents the channel impulse response.

Other features are time dispersion parameters related to impulse response length and mean delay spreading [2]. However, for medical body sensor applications, bit rates are generally less than 10 Mbps but with a high quality of service [7]. We thus only focus on DC gain and neglect intersymbol interference for both IR and VLC channels.

Patient mobility induces different link configurations related to random positions and orientations of the VLC receiver and IR emitter. Consequently, the optical DC gain is a random variable so that channel behavior will be analyzed from statistical distributions. More precisely, we will evaluate its cumulative density function (CDF) defined as

$$\mathrm{CDF}(H_0) = \int_{-\infty}^{H_0} p(H)dH, \tag{3}$$

where $\mathrm{CDF}(H_0)$ represents the probability that the channel gain is lower than a given value H_0. Therefore, since the system reliability is increased when reaching the highest possible DC gain values with the highest probability, it is thus worth reaching smallest $\mathrm{CDF}(H_0)$ values for a given H_0. Consequently, in the following, we discuss about the IR and VLC link reliability from the evaluation of $\mathrm{CDF}(H_0)$.

4.1. Channel Modeling Approach. To determine the channel impulse response, we adopt a modeling approach based on a stochastic Monte Carlo (MC) method, associated with the ray-tracing (RT) algorithm. Such MCRT approaches first proposed in [34] allow the evaluation of impulse response in the case of complex scenes even considering a large number of reflections. It consists in launching a given number of rays in random directions over the scene, based on a given statistical distribution. Each ray is tracked until it reaches the detector. For simulation time purpose and complexity, a maximal number of reflections per optical beams can be set.

We use the MCRT method in this work for both IR and visible channel modeling. Our research laboratory has developed the RaPSor software (Ray Propagation Simulator), which is an open source and extensible tool, based on the NetBeans platform for modeling optical links [35, 36]. It offers the use of two simulation algorithms: ray shooting (RS) and ray gathering (RG). They are each based on formulations resolved by the method of MC and incorporate optimization techniques to reduce computing time. In the case of the RS method, the rays are launched from the transmitter while the RG method consists in generating rays from the receiver.

Due to patient mobility inside the room, we use here MCRT simulations with RS algorithm to obtain a set of impulse responses $h(t)$ corresponding to different IR and VLC links. We use 10,000 links corresponding to random positions of IR/VLC transceivers since we have verified that this produces convergent results. For all the simulations, in order to manage trade-offs between calculation times and accuracy, we limit number of reflections to three, considering only the optical beams having at maximum three reflections, which is a classical approach for nondirected LOS transmissions. Furthermore, Behlouli et al. [36] showed that objects present in the scene have a weak impact on the link performance for low bit rates. Thus, for simplicity and without loss of generality, we do not model furniture and set the room surface reflection coefficients equal to 0.8 corresponding to the classical value for standard walls and ceiling [36]. Consequently, we consider that the main element affecting optical beam propagation is the patient's body.

To study the impact of the human body on an optical channel, we have to model its geometry and its reflectance properties. We have shown previously that level of detail is not important for evaluating channel DC gain when considering low data rates [36]. Consequently, we will use the 3D body model presented in Figure 4. The height of the body is set to 1.7 m and its width to 20 cm. We investigate different sensor positions between the ankle location at $H_T = 0.2$ m from the floor and the shoulder location corresponding to $H_T = 1.5$ m. We also consider a position at the top of the body with $H_T = 1.7$ m.

A human body surface is composed of two main parts: skin and clothing. These surfaces can add reflecting or absorbing effects to the optical propagation. As there is a large range of body reflectivity values [37], we investigate in the following the importance of a precise value of ρ for both IR and VLC channels.

4.2. IR Channel Behavior. To determine the DC gain $H_{0\text{–IR}}$ for infrared uplink, we define H_i as being the DC gain between $\mathrm{T_{X\text{-}IR}}$ and the receiver $\mathrm{R_{X\text{-}IR\text{-}}}i$ with i varying from 1 to 4. The emitter $\mathrm{T_{X\text{-}IR}}$ is characterized by a given position and orientation. Taking into account the SwC method, we determine $H_{0\text{–IR}}$ as the best gain considering the four active receivers:

$$H_{0\text{–IR}} = \mathrm{Max}[H_1, H_2, H_3, H_4]. \tag{4}$$

As the patient position is random within the environment, $H_{0\text{–IR}}$ follows a statistical distribution $p(H_{\mathrm{IR}})$. The CDF of the gain $H_{0\text{–IR}}$ can be thus expressed as

$$\mathrm{CDF}(H_{0\text{–IR}}) = \int_{-\infty}^{H_{0\text{–IR}}} p(H_{\mathrm{IR}})dH_{\mathrm{IR}}. \tag{5}$$

Figure 5 shows the CDF obtained according to the $\mathrm{T_{X\text{-}IR}}$ positions on the body defined by the height H_T. These

Table 2: IR uplink parameters.

	Parameter	Value
$T_{X\text{-}IR}$	Height H_T from the floor	Variable between [0.2–1.7] (m)
	Polar angle θ	Random in $[0, \pi/3]$, with a step of $\pi/6$
	Azimuthal angle φ	Random in $[0, \pi]$, with a step of $\pi/6$
$R_{X\text{-}IR\text{-}i}$	Coordinates $[x, y, z]$	$i = 1$: [3.05, 3, 2.8] (m)
		$i = 2$: [3.05, 3.6, 2.8] (m)
		$i = 3$: [3.65, 3, 2.8] (m)
		$i = 4$: [3.65, 3.6, 2.8] (m)
	Orientation at each corner of the panel	45°
	Field-of-view (FOV)	45°
	Physical surface area	34.5 mm^2
	Responsivity	1 A/W

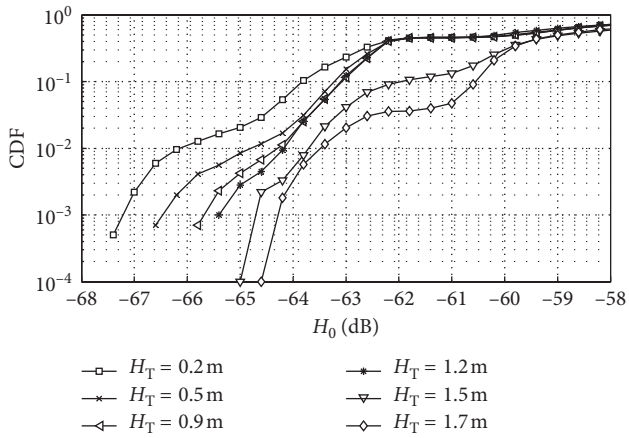

Figure 5: Cumulative density function of $H_{0\text{–IR}}$ for several $T_{X\text{-IR}}$ positions on the body ($\rho = 0.1$) defined by the height H_T.

locations could correspond to the ankle, knee, wrist, shoulder, and head. The body reflectivity is set to $\rho = 0.1$. We observe that performance deteriorates when the height H_T is small. The results show that the presence of the body has a significant impact if the transmitter is located at a height less than 1.5 m above the floor. Therefore, it is important to model the presence of the body to avoid underestimating the performance of IR communication.

To estimate the impact of body as a function of its optical properties, Figure 6 shows the CDF of the gain as a function of ρ for two extreme positions, one near the ground at the ankle ($H_T = 0.2$ m) and the other at the shoulder ($H_T = 1.5$ m).

In Figure 6, we observe the influence of ρ on the DC gain values corresponding to the smaller CDFs. The gain values degrade as ρ decreases for the two positions studied. We can note, however, that the value of ρ has a smaller effect when the sensor is on the shoulder than when it is at the ankle.

To complete the analysis, we study the impact of polar and azimuthal angles representing changes of orientations of the transmitter related to the movements of the patient. The results are shown in Figure 7 for the two previous extreme positions, $H_T = 0.2$ m and $H_T = 1.5$ m. The CDF of the gain is plotted for random values of the angles as defined in Table 2 and for $\varphi = \theta = 0$, corresponding to a fixed orientation towards the ceiling. The number of position is set to 10,000 in both cases since we have verified that the results converge with this number of samples. In random orientation case, with a step of $\pi/6$, this corresponds to 12 samples per position, i.e., 120,000 samples.

Whatever the H_T value, the curves are almost the same whether considering random orientations or not. Within the studied range of angle variations, the channel has the same behavior as when the transmitter is oriented towards the ceiling. Therefore, it is not useful to take into account the changes in orientation of $T_{X\text{-IR}}$. Consequently, the IR channel modeling can be simplified.

4.3. Visible Channel Behavior. The VLC emitter $T_{X\text{-VLC}}$ is at the center of the ceiling and communicates with a receiver $R_{X\text{-VLC}}$ whose characteristics are defined in Table 1. We consider the impact of the position of the receiver in the room because of the mobility of the patient and consider 10,000 links in the simulation. For a given position, we assume that patient movements can induce random changes in receiver orientation modeled by azimuthal and polar angles of φ and θ, respectively, as defined in Table 1. Consequently, the gain $H_{0\text{–VLC}}$ is a random variable and follows a statistical distribution.

We analyze the channel behavior by discussing the evolution of the CDF of the gain $H_{0\text{–VLC}}$. We also study the effects linked to blockage of the link by the patient's body, characterized by the reflectivity coefficient ρ. First, we consider a body with $\rho = 0.1$; the results are provided in Figure 8. The reported CDF corresponds to a scenario taking into account the presence of a body with a receiver $R_{X\text{-VLC}}$ whose orientation is either fixed (perpendicular) or randomly variable. We also plot the results for the case without a body model.

By observing the gain values corresponding to the smallest CDF, we see that when the receiver orientation is fixed perpendicular to the ceiling, the body impact is not significant. This is related to the fact that the receiver is supposed to be placed 20 cm in front of the body. In contrast, the results are highly impacted when the orientation of the receiver is variable. Indeed, in this case, some optical rays cannot be collected by the photodetector FOV. In addition, the body can block them and reflect a part of the rays.

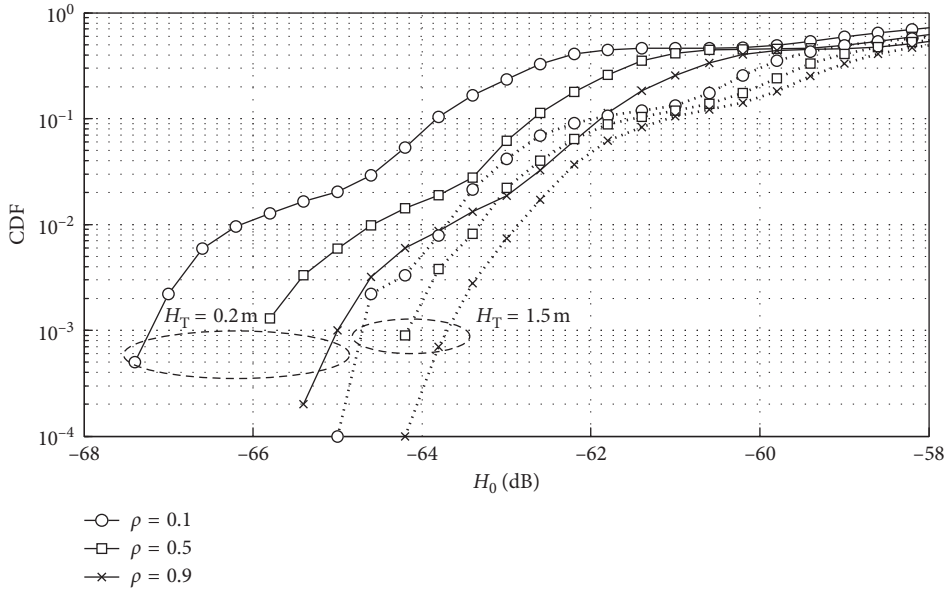

FIGURE 6: Cumulative density function of H_{0-IR} for several body reflectivity coefficients ρ; two $T_{X\text{-}IR}$ positions: at the ankle (plain lines) and on the shoulder (dotted lines).

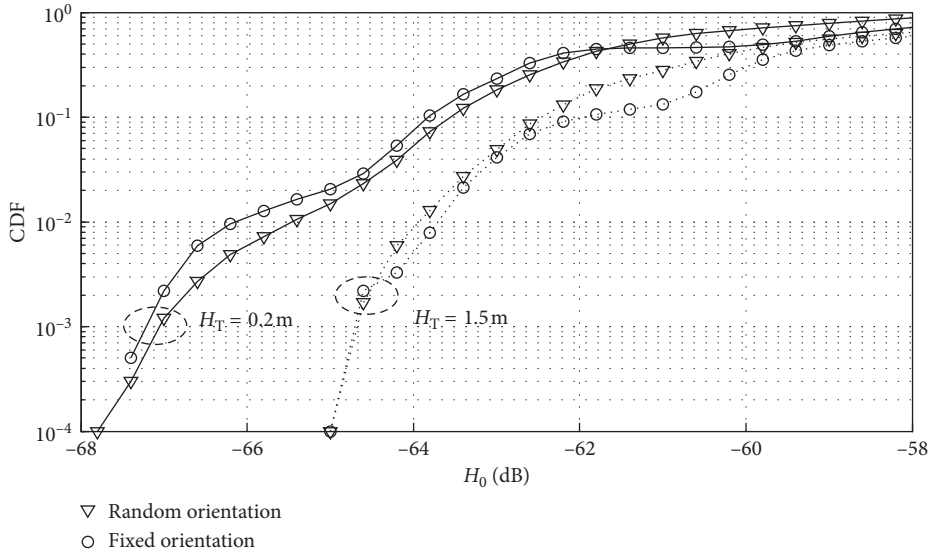

FIGURE 7: Cumulative density function of H_{0-IR} for several $T_{X\text{-}IR}$ orientations; two $T_{X\text{-}IR}$ positions: at the ankle (0.2 m) and on the shoulder (1.5 m); $\rho = 0.1$.

Consequently, for visible downlink channel characterization, it is important to model body presence along with the random orientation of $R_{X\text{-}VLC}$. To complete these results, we studied the impact of the reflectivity value ρ. The results are reported in Figure 9.

As expected, DC gain is degraded when ρ diminishes, in particular, for ρ lower than 0.5. Thus, it can be important to take into account body reflectivity properties while estimating performance.

4.4. Summary on Channel Modeling. Channel behavior was studied with regard to the channel gain variations when a patient moving within the environment wears an IR emitter and a VLC receiver. We found that IR uplink performance depends on the position of the transmitter on the body. Whatever the position, it is not necessary to take into account variations in emitter orientation. However, it is essential to model the body with a reflectivity coefficient value that is as accurate as possible, particularly when the sensor is close to the floor.

With regard to the visible downlink, modeling the body with the knowledge of its optical properties and taking into account VLC receiver orientations variations are key points for the determination of performance.

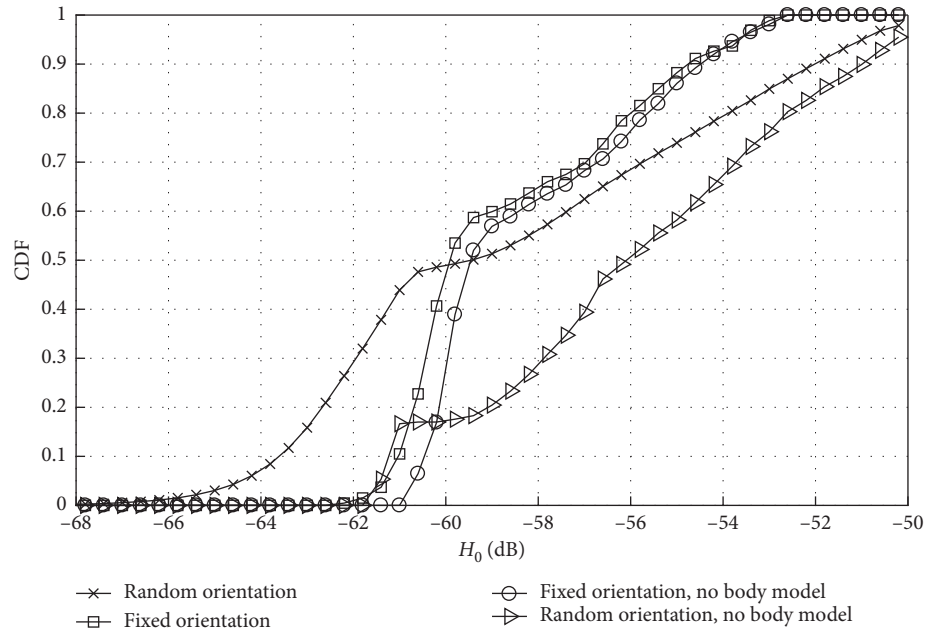

Figure 8: Cumulative density function of $H_{0-\mathrm{VLC}}$; cases with and without body model ($\rho = 0.1$), random and perpendicular orientations of $\mathrm{R}_{\mathrm{X\text{-}VLC}}$.

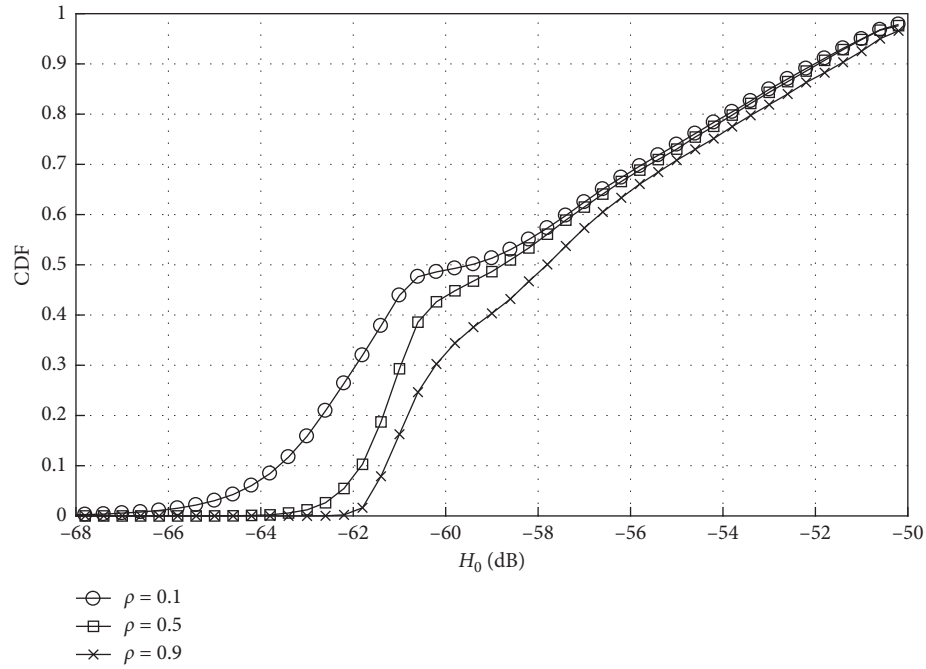

Figure 9: Cumulative density function of $H_{0-\mathrm{VLC}}$ for several values of body reflectivity ρ.

In the next section, we evaluate the overall system performance for body sensor communication taking into account IR and VLC channel models.

5. Performance Results

5.1. Overall Performance Definition. Linked to the channel DC gain H_0 and depending on the system modulation, the signal-to-noise ratio (SNR) is a key metric used to evaluate performance, taking into account emitter power and noise contribution. Considering the on-off keying (OOK) modulation and equiprobable emission, the SNR is given by

$$\mathrm{SNR} = \frac{P_{\mathrm{t}}^2 H_0^2 R^2}{N_0 R_{\mathrm{b}}}, \tag{6}$$

where R_{b} is the data rate, P_{t} is the average optical emitted power, N_0 is the noise power spectral density value

assuming an additive white Gaussian noise (AWGN), and R is the photodiode responsivity.

Noise power is mainly linked to the induced ambient photocurrent I_B by [2]

$$N_0 \approx 2qI_B, \tag{7}$$

where q is the electron quantum charge.

Visible and IR channels are both impacted by ambient noise but the effects are more severe in visible since it shares the same spectrum as lighting sources.

In our context, we have taken account for ambient light source mainly related to background illumination conditions as direct sun light. Other artificial ambient light sources are not supposed to be present as we consider that the communicating LED-based fixture ensures the illumination function. Therefore, we consider in the following analysis values of I_B around 5100 μA for visible link and 200 μA for IR that are values reported from indoor measurements in [38] for several typical ambient light conditions.

Based on the SNR, the bit error rate (BER) is classically used to discuss performance. However, as H_0 follows a statistical distribution because of the patient moving within the environment, the SNR also randomly varies. Therefore, the system BER varies according to the patient's position and the movements of the IR transmitter or the VLC receiver.

To account for these variations, we use a metric based on the probability of meeting a given performance in terms of BER. A given performance corresponds to an SNR limit value called SNR_0. If the SNR is smaller than SNR_0, the targeted performance cannot be reached and the system is in outage. Therefore, we discuss link performance considering the outage probability P_{out} expressed as

$$P_{\mathrm{out}} = p\left(\mathrm{SNR} < \mathrm{SNR}_0\right). \tag{8}$$

As we have seen in the previous section, statistical channel behaviors are different for VLC and IR links. So, we compute two different outage probabilities corresponding to each link and involving pairs of emitted power and data rates (($P_{\mathrm{t-IR}}$, $R_{\mathrm{b-IR}}$) and ($P_{\mathrm{t-VLC}}$, $R_{\mathrm{b-VLC}}$), respectively):

$$\begin{aligned} P_{\mathrm{out-IR}} &= p\left(\mathrm{SNR}_{\mathrm{IR}} < \mathrm{SNR}_{0-\mathrm{IR}}\right), \\ P_{\mathrm{out-VLC}} &= p\left(\mathrm{SNR}_{\mathrm{VLC}} < \mathrm{SNR}_{0-\mathrm{VLC}}\right). \end{aligned} \tag{9}$$

Considering that the system is in outage as soon as one of the links (uplink or downlink) is in outage (defined in relation to a given $\mathrm{SNR}_{0\text{-IR}}$, resp. $\mathrm{SNR}_{0\text{-VLC}}$), we determine the global outage probability to evaluate the system performance as follows:

$$\begin{aligned} P_{\mathrm{out}} &= p\left(\mathrm{SNR}_{\mathrm{IR}} < \mathrm{SNR}_{0-\mathrm{IR}} \cup \mathrm{SNR}_{\mathrm{VLC}} < \mathrm{SNR}_{0-\mathrm{VLC}}\right) \\ &= p\left(\mathrm{SNR}_{\mathrm{IR}} < \mathrm{SNR}_{0-\mathrm{IR}}\right) + p\left(\mathrm{SNR}_{\mathrm{VLC}} < \mathrm{SNR}_{0-\mathrm{VLC}}\right) \\ &\quad - p\left(\mathrm{SNR}_{\mathrm{IR}} < \mathrm{SNR}_{0-\mathrm{IR}}\right) \cdot p\left(\mathrm{SNR}_{\mathrm{VLC}} < \mathrm{SNR}_{0-\mathrm{VLC}}\right) \\ &= P_{\mathrm{out-IR}} + P_{\mathrm{out-VLC}} - P_{\mathrm{out-IR}} \cdot P_{\mathrm{out-VLC}}. \end{aligned} \tag{10}$$

The SNR limit values ($\mathrm{SNR}_{0\text{-IR}}$ and $\mathrm{SNR}_{0\text{-VLC}}$) can be different depending on the target application, for which different kinds of data can be sent in the uplink and downlink.

In this study, we consider that they are fixed to the same value: $\mathrm{SNR}_{0\text{-IR}} = \mathrm{SNR}_{0\text{-VLC}} = 15.6$ dB, corresponding to a BER of around 10^{-9} for OOK modulation. This corresponds to classical on-body sensor links requirements for medical applications [18].

However, we will consider in the analysis that data rates and emitted power are different and the aim is to evaluate which pairs satisfy a targeted global outage probability.

5.2. Results and Discussion. Considering the conclusions of the IR and VLC channels study, the first discussion concerns the overall performance of the IR transmitter for different positions on the body. This analysis can be done for a fixed data rate $R_{\mathrm{b\text{-}IR}} = R_{\mathrm{b\text{-}VLC}}$.

From expression (8), and knowing the SNR distributions for a given system configuration, it is possible to determine which pairs ($P_{\mathrm{t-VLC}}$, $P_{\mathrm{t-IR}}$) generate a given P_{out}. An example is given in Figure 10 for the OOK modulation, with IR and VLC transceiver parameters defined in Tables 1 and 2. Two positions of the IR emitter, $H_T = 0.2$ m and $H_T = 1.5$ m, are studied, assuming body reflectivity $\rho = 0.1$.

We determined the pairs ($P_{\mathrm{t-VLC}}$, $P_{\mathrm{t-IR}}$) for 3 different targeted P_{out} and a data rate of $R_b = 1$ Mbps in VLC downlink and IR uplink. Firstly, regardless of the H_T value, the required VLC or IR powers are higher as the overall P_{out} target weakens. This is consistent with the IR channel behavior with regard to emitter position on the body. In addition, to guarantee a given overall quality of service, if the IR power decreases, the VLC power related to the lighting level of the room must be increased and vice versa. From these curves, we can thus extract the two pairs of limit values for IR and VLC power. For example, for $P_{\mathrm{out}} = 0.1$ and $H_T = 0.2$ m, the first pair of values corresponds to a minimal IR power $P_{\mathrm{t-IR-min}}$ around 83 mW with a maximal VLC power $P_{\mathrm{t-VLC-max}}$ of 0.88 W. The other pair is $P_{\mathrm{t-VLC-min}}$ around 0.39 W with a $P_{\mathrm{t-IR-max}}$ of 161 mW. However, the range of power values is reduced when the target outage probability P_{out} becomes low, i.e., when the quality of service is high.

Next we focus on the sensitive sensor location regarding body impact that is at the ankle $H_T = 0.2$ m. The goal is to show the potential of the proposed technology for this sensor position, the most impacted by body presence.

Figure 11 shows the pairs of values ($P_{\mathrm{t-IR-min}}$, $P_{\mathrm{t-VLC-max}}$) corresponding to 3 different outage probabilities as a function of body reflectivity value ρ for the height $H_T = 0.2$ m.

For $P_{\mathrm{t-IR-min}}$ and $P_{\mathrm{out}} = 0.1$, the reflectivity value ρ does not have a significant impact, whereas the impact is more important when the required outage probability is lower. $P_{\mathrm{t-VLC-max}}$ evolution does not follow the same pattern of behavior. It is not so heavily impacted by the required outage probability, regardless of the reflectivity value ρ. In addition, the reflectivity value has an impact only for ρ values lower than 0.5.

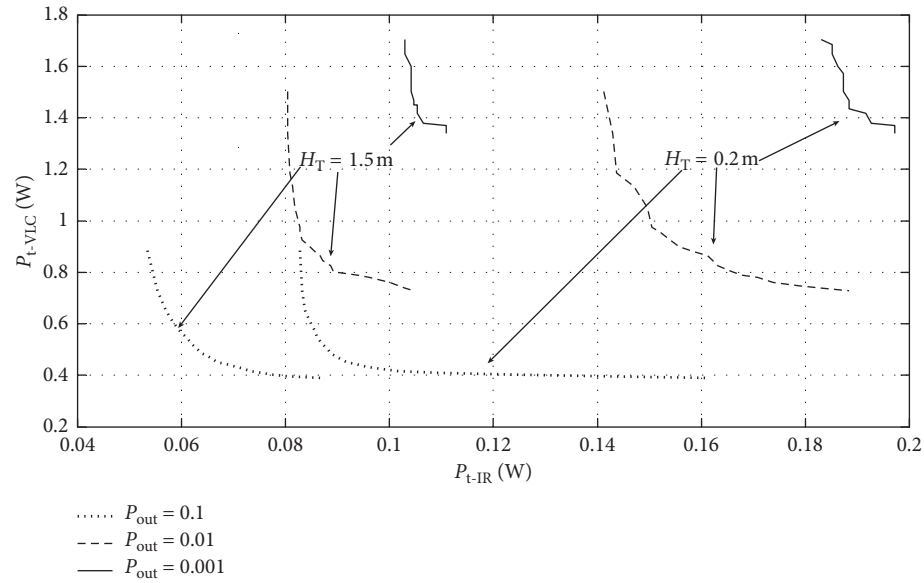

FIGURE 10: Evolution of IR and VLC emitted power for 3 given values of P_{out}; body reflectivity $\rho = 0.1$; height $H_T = 0.2$ m and $H_T = 1.5$ m; data rate $R_b = 1$ Mbps.

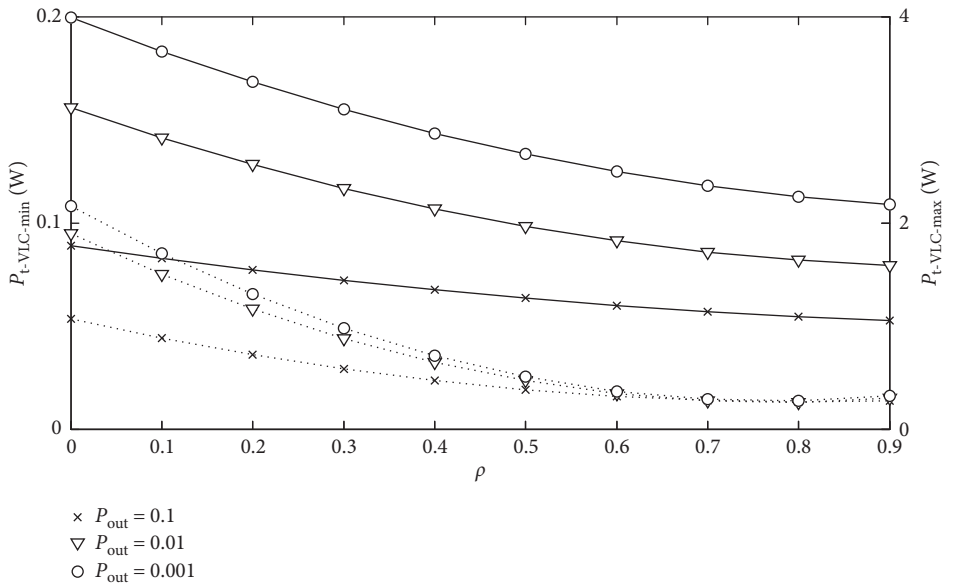

FIGURE 11: Evolution of $P_{\text{t-IR-min}}$ (in plain lines) and $P_{\text{t-VLC-max}}$ (in dotted lines) for 3 given values of P_{out} as a function of body reflectivity ρ; height $H_T = 0.2$ m; data rate $R_b = 1$ Mbps.

For the same configuration, i.e., $H_T = 0.2$ m and for the 3 different targeted outage probabilities, Figure 12 shows the corresponding pairs of values ($P_{\text{t-VLC-min}}$, $P_{\text{t-IR-max}}$).

$P_{\text{t-VLC-min}}$ variations, as for the $P_{\text{t-VLC-max}}$ value, do not depend on reflectivity values when ρ is higher than 0.5. However, for lower ρ values, they vary as a function of ρ and as a function of the required outage probability. We also note that the maximal power $P_{\text{t-IR-max}}$ for the IR link is always lower than the admissive value for IR diffuse radiation considering IEC/EN 60825 standard (around 300 mW [2]). This is of great importance for consumption and highlights the potentiality of this VLC/IR solution for body sensor communication.

Besides, the results indicate that the VLC power is always lower than 2 W. This corresponds to weak illumination, barely perceptible by the human eye, similar to night watch use (around 20 lux [39]). This is important for monitoring applications for which data transmission has to be reliable whatever the lighting conditions.

To extend the conclusions, this analysis can be done for any other data rates, which are not necessarily the same for IR and VLC links. Thus, we analyze the variations of

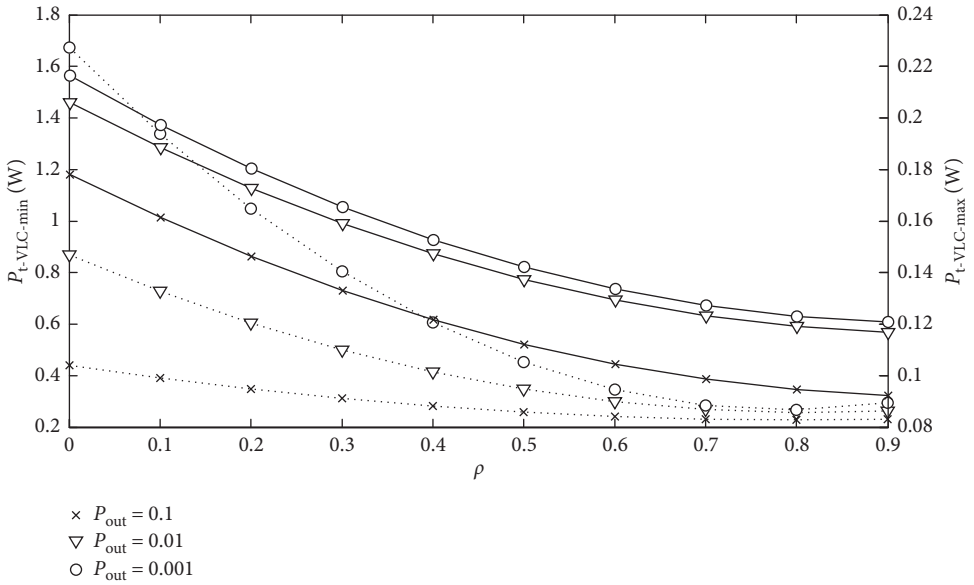

FIGURE 12: Evolution of, $P_{t\text{–}IR\text{–}max}$ (in plain lines) and $P_{t\text{–}VLC\text{–}min}$ (in dotted lines) for 3 given values of P_{out} as a function of body reflectivity ρ; height $H_T = 0.2$ m; data rate $R_b = 1$ Mbps.

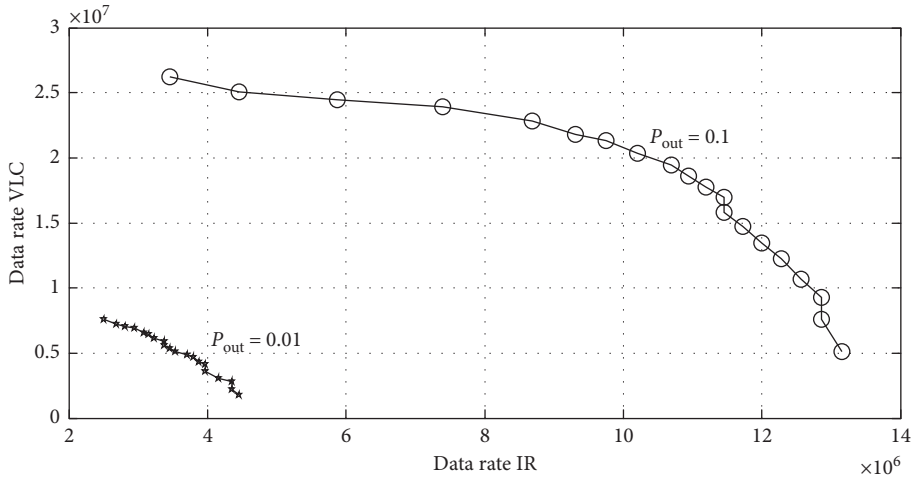

FIGURE 13: Evolution of, data rate for IR and VLC links for 2 given values of P_{out}; $P_{t\text{–}IR} = 300$ mW and $P_{t\text{–}VLC} = 2$ W; body reflectivity $\rho = 0.1$; height $H_T = 0.2$ m.

available data rates to reach a given outage for fixed power values. We consider the case with maximal IR power, i.e., $P_{t\text{–}IR} = 300$ mW. We also assume that $P_{t\text{–}VLC} = 2$ W as in night watch use. Results are shown in Figure 13 for a reflectivity value $\rho = 0.1$ and $H_T = 0.2$ m and for two different levels of quality of service corresponding to $P_{out} = 0.1$ and $P_{out} = 0.01$.

The curves indicate that the proposed system can operate at data rates higher than 1 Mbps. This illustrates the theoretical potential of all-optical communication technology for body-sensor based health monitoring even for extreme position of the sensor on the user body like the ankle. For example, the pairs of maximal data rates for IR and VLC are ($R_{b\text{–}IR\text{–}max} = 13.2$ Mbps, $R_{b\text{–}VLC\text{–}max} = 26$ Mbps) for $P_{out} = 0.1$ and ($R_{b\text{–}IR\text{–}max} = 4.5$ Mbps, $R_{b\text{–}VLC\text{–}max} = 7.5$ Mbps) for $P_{out} = 0.01$. As expected, the range of data rate is reduced when the targeted outage probability is lower.

6. Conclusion

In this work, we proposed a bidirectional all-optical communication system using infrared uplink and visible downlink. The context is body sensor communications for medical applications. The studied scenario considered an infrared communicating sensor worn by a patient and associated receivers positioned in a ceiling luminaire. This luminaire can communicate in the visible range with a receiver also worn by the patient.

Performance was analyzed taking into account the main impacting parameters, i.e., the movements and the mobility

of the patient in the environment, the position of the communicating sensor on his/her body, and the presence of the body and its impact on optical propagation.

First, we analyzed the statistical behavior of both IR and VLC channels using ray-tracing simulations, allowing modeling of LOS and non-LOS links.

The results showed that regardless of the position of the communicating sensor on the body, it is not necessary to take into account variations in orientation of the infrared emitters, which simplifies the modeling. However, it is essential to model the body with a reflectivity coefficient value as close to reality as possible, especially when the sensor is close to the ground, for example, at the ankle. In contrast, for the visible downlink channel, it is important not only to model the body but also the variations in orientation of the VLC receivers.

Then, the channel statistics were used to determine the overall performance in terms of outage probability, jointly considering IR uplink and visible downlink transmissions.

First, we focused on a scenario with a data rate of 1 Mbps and BER of 10^{-9} for both links. The analysis of overall performance was done by examining the emitting power-related issues. We determined the compromises required in IR and VLC powers to satisfy a given quality of service. Thus, the minimum power possible in infrared will correspond to a maximum power in visible and vice versa.

An important result is that even with an ankle sensor, the maximum power for the uplink did not exceed the maximum permissible value in IR diffuse emission. Moreover, when the IR emitted power was minimized, the corresponding maximum VLC power did not depend on the quality of service or body reflectivity when it was greater than 0.5. This was the same when considering minimal VLC power regarding body reflectivity. We also found that VLC maximal power corresponds to a very low level of illumination, so the application does not depend on lighting conditions.

Finally, we determined the maximum rates for which these conclusions are still valid, which shows the potentialities of optical wireless technology in a body sensor context.

Data Availability

The data used to support the findings of this study are included within the article and are available from the corresponding author upon request.

Conflicts of Interest

The authors declare that they have no conflicts of interest.

Acknowledgments

This study was supported in part by the Partnership Foundation of Limoges University, France.

References

[1] S. Arnon, J. Barry, G. K. Karagiannidis, R. Schober, and M. Uysal, *Advanced Optical Wireless Communication Systems*, Cambridge University Press, New York, NY, USA, 1st edition, 2012.

[2] Z. Ghassemloy, W. Popoola, and S. Rajbhandari, *Optical Wireless Communications: System and Channel Modeling with MATLAB®*, CRC Press, Boca Raton FL, USA, 1st edition, 2012.

[3] D. Karunatilaka, F. Zafar, V. Kalavally, and R. Parthiban, "LED based indoor visible light communications: state of the art," *IEEE Communications Surveys & Tutorials*, vol. 17, no. 3, pp. 1649–1678, 2015.

[4] S. Arnon, *Visible Light Communication*, Cambridge University Press, New York, NY, USA, 1st edition, 2015.

[5] S. Dimitrov and H. Haas, *Principles of LED Light Communications towards Networked Li-Fi*, Cambridge University Press, Cambridge, UK, 1st edition, 2015.

[6] Z. Ghassemlooy, L. N. Alves, S. Zvanovec, and M.-A. Khalighi, *Visible Light Communications: Theory and Applications*, CRC Press, Boca Raton, FL, USA, 1st edition, 2017.

[7] A. Julien-Vergonjanne, S. Sahuguede, and L. Chevalier, "Optical wireless body area networks for healthcare applications," in *Optical Wireless Communications: An Emerging Technology*, M. Uysal, C. Capsoni, Z. Ghassemlooy, A. Boucouvalas, and E. Udvary, Eds., pp. 569–587, Springer International Publishing, Basel, Switzerland, 1st edition, 2016.

[8] B. C. Pedersen, *Medical Electrical Equipment, IEC 60601-1-2, Part 1-2*, IEC, Geneva, Switzerland, 2014.

[9] T. Cogalan and H. Haas, "Why would 5G need optical wireless communications?," in *Proceedings of the IEEE 28th Annual International Symposium on Personal, Indoor, and Mobile Radio Communications (PIMRC)*, pp. 1–6, Montreal, Canada, October 2017.

[10] IEC 60825-1, *Safety of Laser Products—Part 1 Equipment Classification and Requirement*, IEC, Geneva, Switzerland, 2007.

[11] IEC 62471, *Photo-biological Safety of Lamps and Lamp Systems (Identical with CIE S009)*, IEC, Geneva, Switzerland, 2006.

[12] ISO/IEEE international standard health informatics—Point-of-care medical device communication—Transport profile—Infrared," in *ISO/IEEE 11073-30300:2004*, IEEE, Piscataway, NJ, USA, 2004.

[13] S. S. Torkestani, S. Sahuguede, A. Julien-Vergonjanne, and J. P. Cances, "Indoor optical wireless system dedicated to healthcare application in a hospital," *IET Communications*, vol. 6, no. 5, pp. 541–547, 2012.

[14] S. S. Torkestani, S. Sahuguede, A. Julien-Vergonjanne, J. Cances, and J. C. Daviet, "Infrared communication technology applied to indoor mobile healthcare monitoring system," *International Journal of E-Health and Medical Communications*, vol. 3, no. 3, pp. 1–11, 2012.

[15] A. M. Khalid, G. Cossu, and E. Ciaramella, "Diffuse IR-optical wireless system demonstration for mobile patient monitoring in hospitals," in *Proceedings of the 15th International Conference on Transparent Optical Networks (ICTON)*, pp. 1–4, Cartagena, Spain, June 2013.

[16] P. Toumieux, S. Sahuguède, L. Chevalier, and A. Julien-Vergonjanne, "Optical wireless connected objects for healthcare," *Healthcare Technology Letters*, vol. 2, no. 5, pp. 118–122, 2015.

[17] E. A. Alyan and S. A. Aljunid, "Development of wireless optical CDMA system for biosignal monitoring," *Optik*, vol. 145, pp. 250–257, 2017.

[18] L. Chevalier, S. Sahuguede, and A. Julien-Vergonjanne, "Optical wireless links as an alternative to radio-frequency for

medical body area networks," *IEEE Journal on Selected Areas in Communications*, vol. 33, no. 9, pp. 2002–2010, 2015.

[19] Y.-K. Cheong, X.-W. Ng, and W.-Y. Chung, "Hazardless biomedical sensing data transmission using VLC," *IEEE Sensors Journal*, vol. 13, no. 9, pp. 3347-3348, 2013.

[20] D. R. Dhatchayeny, A. Sewaiwar, S. V. Tiwari, and Y. H. Chung, "EEG biomedical signal transmission using visible light communication," in *Proceedings of the 2015 International Conference on Industrial Instrumentation and Control (ICIC)*, pp. 243–246, Pune, India, May 2015.

[21] A. Al-Qahtani, H. Al-hajri, S. Al-kuwari et al., "A non-invasive remote health monitoring system using visible light communication," in *Proceedings of the 2015 2nd International Symposium on Future Information and Communication Technologies for Ubiquitous HealthCare (Ubi-HealthTech)*, pp. 1–3, Beijing, China, May 2015.

[22] W. A. Cahyadi, T.-I Jeong, Y.-H Kim, Y.-H Chung, and T. Adiono, "Patient monitoring using visible light uplink data transmission," in *Proceedings of the 2015 International Symposium on Intelligent Signal Processing and Communication Systems (ISPACS)*, pp. 431–443, Nusa Dua, Indonesia, November 2015.

[23] W. Noonpakdee, "Performance analysis of passive—Active optical wireless transmission for personal health monitoring," in *Proceedings of the 2014 Sixth International Conference on Ubiquitous and Future Networks (ICUFN)*, pp. 17–21, Shanghai, China, July 2014.

[24] V. P. Rachim, J. An, P. N. Quan, and W.-Y Chung, "A novel smartphone camera-LED communication for clinical signal transmission in mhealth-rehabilitation system," in *Proceedings of the 2017 39th Annual International Conference of the IEEE Engineering in Medicine and Biology Society (EMBC)*, pp. 3437–3440, Seogwipo, South Korea, July 2017.

[25] Y. Y. Tan and W. Y. Chung, "Mobile health-monitoring system through visible light communication," *Bio-Medical Materials and Engineering*, vol. 24, no. 6, pp. 3529–3538, 2014.

[26] C. R. Uma Kumari and S. Dhanalakshmi, "All optical health monitoring system: an experimental study on visible light communication in biomedical signal transmission," in *Innovations in Electronics and Communication Engineering*, H. S. Saini, R. K. Singh, and K. Satish, Eds., pp. 361–370, Springer, Singapore, 2018.

[27] C. L. Bas, T. B. Hoang, S. Sahuguede, and A. Julien-Vergonjanne, "Lighting fixture communicating in infrared and visible for indoor health monitoring," in *Proceedings of the 2017 IEEE 19th International Conference on e-Health Networking, Applications and Services (Healthcom)*, pp. 1–6, Dalian, China, October 2017.

[28] A. Hadjidj, M. Souil, A. Bouabdallah, Y. Challal, and H. Owen, "Wireless sensor networks for rehabilitation applications: challenges and opportunities," *Journal of Network and Computer Applications*, vol. 36, no. 1, pp. 1–15, 2013.

[29] T. B. Hoang, S. Kandukuri, S. Sahuguede, and A. Julien-Vergonjanne, "Infrared mobile transmissions for smart indoor applications," in *Proceeding sof the 2018 11th International Symposium on Communication Systems, Networks & Digital Signal Processing (CSNDSP)*, pp. 1–6, Budapest, Hungary, July 2018.

[30] H. Ma, L. Lampe, and S. Hranilovic, "Integration of indoor visible light and power line communication systems," in *Proceedings of the 2013 IEEE 17th International Symposium on Power Line Communications and its Applications*, pp. 291–296, Johannesburg, South Africa, March 2013.

[31] T. B. Hoang, S. Sahuguede, and A. Julien-Vergonjanne, "Behavior of non-directed optical wireless channel considering receiver orientation"," in *Proceedings of the 2017 20th International Symposium on Wireless Personal Multimedia Communications (WPMC)*, pp. 223–228, Bali, Indonesia, December 2017.

[32] D. Wu, Z. Ghassemlooy, W.-D. Zhong et al., "Effect of optimal Lambertian order for cellular indoor optical wireless communication and positioning systems," *Optical Engineering*, vol. 55, no. 6, Article ID 066114, 2016.

[33] A. Goldsmith, *Wireless Communications*, Cambridge University Press, Cambridge, UK, 2005.

[34] F. J. López-Hernández, R. Pérez-Jiménez, and A. Santamaria, "Monte Carlo calculation of impulse response on diffuse IR wireless indoor channels," *Electronics Letters*, vol. 34, no. 12, pp. 1260–1262, 1998.

[35] A. Behlouli, P. Combeau, and L. Aveneau, "MCMC methods for realistic indoor wireless optical channels simulation," *Journal of Lightwave Technology*, vol. 35, no. 9, pp. 1575–1587, 2017.

[36] A. Behlouli, P. Combeau, S. Sahuguede, A. Julien-Vergonjanne, C. L. Bas, and L. Aveneau, "Impact of physical and geometrical parameters on visible light communication links," in *Proceedings of the 2017 Advances in Wireless and Optical Communications (RTUWO)*, pp. 73–79, Riga, Latvia, November 2017.

[37] A. S. Glassner, *Principles of Digital Image Synthesis*, Morgan Kaufman, San Francisco, CA, USA, 1994.

[38] A. J. C. Moreira, R. T. Valadas, and A. M. de Oliveira Duarte, "Characterization and modelling of artificial light interference in optical wireless communication systems," in *Proceedings of the IEEE International Symposium on Personal Indoor Mobile Radio Communication (PIMRC)*, pp. 326–331, Toronto, Canada, September 1995.

[39] C. Lebas, S. Sahuguede, A. Julien-Vergonjanne, P. Combeau, and L. Aveneau, "Infrared and visible links for medical body sensor networks," in *Proceedings of the Global LIFI Congress (GLC)*, pp. 1–6, Paris, France, February 2018.